Optics Letters

Meter-scale spatial-resolution-coherent Doppler wind lidar based on Golay coding

Chong Wang,[1,2] Haiyun Xia,[1,2,*] Yunbin Wu,[1,2] Jingjing Dong,[2] Tianwen Wei,[1] Lu Wang,[1] and Xiankang Dou[1]

[1]CAS Key Laboratory of Geospace Environment, University of Science and Technology of China, Hefei 230026, China
[2]Glory China Institute of Lidar Technology, Shanghai 201315, China
*Corresponding author: hsia@ustc.edu.cn

Received 5 November 2018; revised 4 December 2018; accepted 5 December 2018; posted 6 December 2018 (Doc. ID 350058); published 9 January 2019

Generally, the pulse duration of a coherent Doppler wind lidar (CDWL) is shortened to minimize the spatial resolution at the sacrifice of carrier-to-noise ratio, since the peak power of a laser source is limited by the stimulated Brillouin scattering or other nonlinear optical phenomena. To solve this problem, an all-fiber CDWL incorporating Golay coding is proposed and demonstrated. Given the peak power of the laser pulse, the Golay coding method can improve the measuring precision by improving the pulse repetition frequency of the outgoing laser. In the experiment, the Golay coding implementation is optimized by normalizing the intensity of every single pulse of the outgoing laser with a closed-loop feedback, achieving a spatial resolution of 6 m and a temporal resolution of 2 s with a maximum detection range of 552 m. The wind profile in line of sight and the result derived from another noncoding CDWL show good agreement.

https://doi.org/10.1364/OL.44.000311

Doppler wind lidar (DWL) with an all-fiber structure is developed rapidly due to its inherited characteristics, such as high spatial/temporal resolution, high precision, large dynamic range, strong immunity to electromagnetic (EM) interference, and its stability in harsh environments. DWL has been used widely in different applications and scientific researches, such as aviation safety, air force operation in a carrier, wind power generation, and forecast of extreme weather events. Although DWL is mature and commercially available, minimizing the spatial resolution is still a great challenge [1–7].

In order to improve the aviation safety and optimize the aerodynamic design of an aircraft, the impact of small-scale turbulence on aircraft is receiving increasing attention. Aircraft vortex and wakes have also become a serious limitation in managing the efficiency and capacity of airports [8]. The wingspan of the aircraft is about tens of meters. In such a scale, to study and estimate the dynamic influence of the surrounding atmospheric environment (small-scale turbulence, aircraft vortex, and wakes) on the aircraft, DWL with meter-scale spatial resolution is highly demanded.

The spatial resolution (ΔR) of a lidar based on the time-of-flight method is defined as $\Delta R = c\Delta T/2$, where ΔT is the duration [full width at half-maximum (FWHM)] of the transmitted laser pulse. c is the speed of light in the atmosphere. The lidar equation is used to describe the relationship between the backscatter signal, transmitted laser, and atmosphere, and it is defined as [9]

$$P_s(R) = \eta_R \eta_T T^2 E_T \frac{\beta c}{2} \frac{A_r}{R^2}, \tag{1}$$

where $P_s(R)$ is the power of the backscatter signal at a distance of R, E_T is the energy of a single laser pulse, η_T is the transmitter optical efficiency, η_R is the receiver optical efficiency, and T is the single-pass transmittance of laser in atmosphere. β is the aerosol backscattering coefficient, and A_r is the effective area of the telescope. In principle, the following three problems limit the spatial resolution improvement of a lidar:

(1) In coherent Doppler wind lidar (CDWL), the carrier-to-noise ratio (CNR) is proportional to ΔT with a matched filter, where the bandwidth is defined as $B = 1/\Delta T$. Then, the CNR equation is expressed as [9]

$$\mathrm{CNR}(R) = \frac{\eta_h \eta_R \eta_T \lambda E_T \beta T^2 A_r \Delta T}{2hR^2}, \tag{2}$$

where η_h is the heterodyne efficiency, λ is the wavelength, and h is the Plank constant. In order to guarantee the same CNR, lager E_T should be used for compensating a shorter ΔT.

(2) As Eq. (1) shows, $P_s(R)$ is proportional to E_T. The relationship between the laser peak power P_{peak} and E_T is $P_{\mathrm{peak}} = E_T/\Delta T$. But, the power of the laser in the fiber is limited due to nonlinear optical phenomena, particularly the stimulated Brillouin scattering (SBS). According to the equation of SBS threshold power (SBSTP) [10,11],

$$P_{\mathrm{th}} = G_{\mathrm{th}} A_{\mathrm{eff}} / g_B L_{\mathrm{eff}}, \tag{3}$$

where G_{th} is the Brillouin exponential threshold gain factor, A_{eff} is the effective cross-sectional area of a fiber, g_B is the Brillouin gain factor, and L_{eff} is the effective length of the fiber.

The performance of a fiber laser will deteriorate if the laser peak power exceeds P_{th}. For example, the laser pulse may deviate from a Gaussian shape in the trailing edge, causing distortion of the power spectra in Doppler shift inversion.

(3) According to Levin's estimation, the CDWL velocity variance can be reduced by using pulse accumulation [12]. Given a temporal resolution, for better performance, the pulse repetition frequency f_{rep} needs to be increased. But a lidar based on the time-of-flight method has its inherent ambiguity distance defined as $R_{max} = c/(2f_{rep})$. To guarantee a long detection range, the f_{rep} is limited.

To solve the above three problems, much effort has been dedicated to developing a fiber laser with high peak power and short pulse duration. The French Aerospace Lab (ONERA) improves the fiber laser's SBSTP by using large-mode-area fiber or adding special stress to the erbium-doped fiber [13–15]. Their CDWL is designed for long-range detection, where the spatial resolution is 200 m. As far as we know, by using commercial fiber lasers, the minimum spatial resolution of a direct-detection DWL and a CDWL is 11.5 m and 15 m, respectively [7,16].

Recently, the pulse coding technology used in communication has been adopted in optical fiber sensing [17,18], ranging lidar [19], and radar [20]. By using the appropriate pulse coding algorithm, one cannot only improve the performance of the lidar by increasing the f_{rep}, but also enhance the spatial resolution without distance ambiguity. In this Letter, a meter-scale spatial resolution CDWL based on the Golay pulse coding algorithm is demonstrated. The pulse duration is set to be 40 ns, corresponding to a spatial resolution of 6 m.

The setup of the Golay coding CDWL is shown as Fig. 1. A bistatic configuration is used to avoid the reflections from the telescope. The double-"D"-shaped telescope minimizes the blind detection range to 12 m. The continuous-wave (CW) laser from the seed laser is split into an outgoing laser and local oscillator. The arbitrary wave generator (AWG) sends an electrical coding sequence to drive two electro-optic modulators (EOM). In order to realize a high extinction ration, EOM_1 and EOM_2 are synchronized in cascade by tuning the time delay between two output channels of the AWG. After intensity modulation, the CW is chopped into a Golay code pulse sequence and amplified by the EDFA. A small portion of the coded laser is split out and monitored by a high-speed analog detector. Then, the energy of each laser pulse is fed back to the AWG to normalize the Golay coded pulse, constituting a closed-loop control. The local oscillator is frequency-shifted 80 MHz by the acoustic–optic modulator (AOM). The

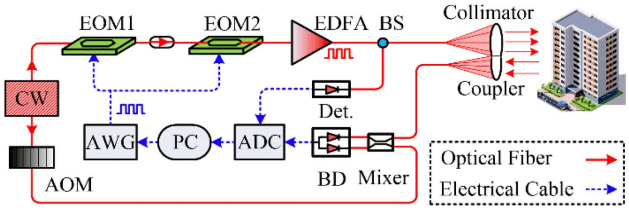

Fig. 1. Optical layout of the Golay coding CDWL. CW, continuous-wave laser; AOM, acoustic–optic modulator; EOM, electro-optic modulator; AWG, arbitrary pulse generator; EDFA, erbium-doped fiber amplifier; BS, beam splitter; BD, balanced detector; ADC, analog-to-digital converter.

Table 1. Key Parameters of the Golay Coding CDWL and Noncoding CDWL

Item	Golay Coding CDWL	Noncoding CDWL
Wavelength	1550 nm	1550 nm
EDFA power	1 W	1.2 W
Pulse duration	40 ns	128 ns
Pulse repetition	3.2 MHz	40 KHz
Spatial resolution	6 m	19.2 m
Temporal resolution	2 s	2 s
Diameter of collimator	100 mm	100 mm
Diameter of coupler	80 mm	80 mm
AOM frequency shift	80 MHz	80 MHz
AOM extinction ratio	—	80 dB
EOM extinction ratio	40 dB	—
Sample rate	500 MS/s	250 MS/s

transmitted laser is sent to the atmosphere by a collimator. The backscatter signal is collected by the coupler and mixed with the local oscillator. A balanced detector and an analog-to-digital converter convert the optical signal to an analog electrical signal. Finally, the signal is stored and processed by using a PC.

The power spectra of the Golay coding CDWL are accumulated over 2 s. The main parameters are listed in Table 1. For comparison, a noncoding CDWL is also built in this work.

Golay code has lots of advantages, such as its pseudorandom sequence, low sidelobes in autocorrelation, and ease of generation. With a bipolar code sequence, it can be used in electronic communication directly. But, in lidar applications, only a unipolar optical pulse can be used. A bipolar Golay code sequence can be transformed to a unipolar optical pulse sequence by the following equations [21]:

$$U_k(t) = [1 + A_k(t)]/2, \quad \bar{U}_k(t) = [1 - A_k(t)]/2,$$
$$W_k(t) = [1 + B_k(t)]/2, \quad \bar{W}_k(t) = [1 - B_k(t)]/2, \tag{4}$$

where $U_k(t), \bar{U}_k(t), W_k(t), \bar{W}_k(t)$ is the unipolar transmitted laser pulse sequence; they are sent one after the other, and four sequences consist of a complete Golay code sequence. $A_k(t), B_k(t)$ is the bipolar Golay code.

The decoding process is shown as Fig. 2. The algorithm of decoding can be described as

$$\mathrm{PSD}(f,t) = \mathrm{corr}\langle [S_{U_k}(f,t) - S_{\bar{U}_k}(f,t)], A_k(t)\rangle + \mathrm{corr}\langle [S_{W_k}(f,t) - S_{\bar{W}_k}(f,t)], B_k(t)\rangle, \tag{5}$$

where $S_{U_k}(f,t), S_{\bar{U}_k}(f,t), S_{W_k}(f,t), S_{\bar{W}_k}(f,t)$ are the backscattering power spectra. Ideally, $S_{U_k}(f,t) = S_p * U_k$, S_p is the backscattering power spectrum of a single pulse. "corr"

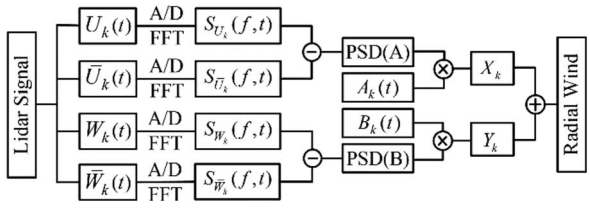

Fig. 2. Decoding process of the Golay coding CDWL, where "⊗" represents the correlation operator.

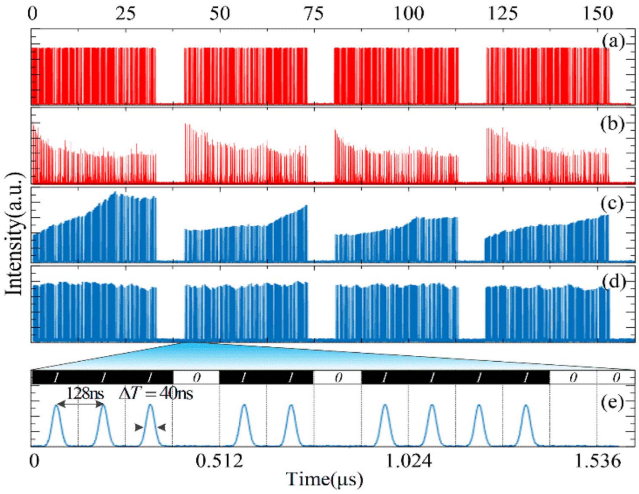

Fig. 3. Laser pulse sequence. (a) Golay coding seed laser and (b) amplified laser sequence without feedback control; (c) Golay coding seed laser; (d) amplified laser sequence with feedback control; (e) enlarged waveform of (d).

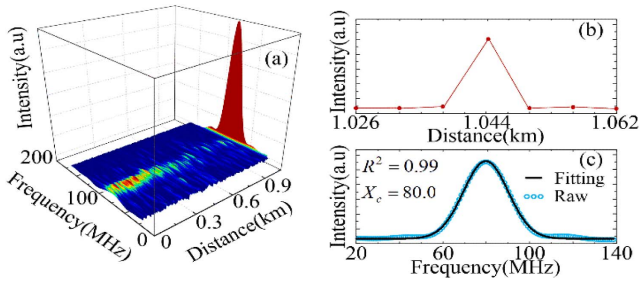

Fig. 4. (a) Power spectra of backscatter signals from atmosphere and a building; (b) the peak of the power spectrum around the hard target; (c) the raw power spectrum of the hard target (blue circle) and its Gaussian fitting curve (black line); the peak of the Gaussian curve is 80.03 MHz.

and "$*$" are correlation and convolution operation, respectively. $\mathrm{PSD}(f,t)$ is the decoded power spectrum, which is similar to the traditional CDWL's power spectrum.

If a long, flat Golay coding seed laser sequence is injected into the EDFA, the power of the amplified Golay coding laser pulse sequence is not flat because of the transient effect and pump exhaustion [22]. Figures 3(a) and 3(b) are the 256 bit Golay coding seed laser pulse sequence and its amplified results without feedback control, respectively.

Considering the nonflat amplified condition, Eq. (5) can be rewritten as

$$\mathrm{PSD}(f,t) = \mathrm{corr}\langle[S_P * (U_k \cdot \beta_{U_k}) - S_P * (\tilde{U}_k \cdot \beta_{\tilde{U}_k})], A_k(t)\rangle + \mathrm{corr}\langle[S_P * (W_k \cdot \beta_{W_k}) - S_P * (\tilde{W}_k \cdot \beta_{\tilde{W}_k})], B_k(t)\rangle, \quad (6)$$

where β is the normalized pulse intensity variation factor. Ideally, $\beta = 1$, and every transmitted pulse should be equal. But, in fact, β is not stable. If $A_k(t)$ and $B_k(t)$ are used to decode the Golay coding signal, serious sidelobes and cross talk between pulses will be introduced, which will induce a low CNR and even fail to retrieve the Doppler shift.

In fiber sensing technology, preamplification of the seed laser [23] or pre-exhaustion of the EDFA [21] is used to solve the nonflat amplified problem. These solutions will either waste the power of the EDFA or are not suitable for high-power EDFA. In this work, an adaptive pulse modification algorithm is demonstrated. When the EDFA is at high population inversion, the input seed laser power will be turned down. At the end of the Golay coding pulse sequence, the EDFA is at low population inversion and nearly exhausted, and the input seed laser power is increased. By using the feedback algorithm, the fluctuation of the amplified laser pulse will be mitigated. Figures 3(c) and 3(d) are the modulated seed and its amplified laser pulse sequence, and the fluctuation is within $\pm 5\%$.

In this coding CDWL, the length of the Golay code sequence is optimized as 256. As shown in Fig. 3(e), the laser pulse repetition frequency is set to be 3.2 MHz; the pulse duration is 40 ns; the temporal window of the fast Fourier transform (FFT) is 40 ns, corresponding to 20 sample points; and the minimum time interval between two pulses is 128 ns.

A wind velocity measurement experiment is carried out on the campus (N31°50′37″, E117°15′54″). The spatial and temporal resolution of the Golay coding CDWL are 6 m and 2 s, respectively. In order to verify the correctness of the results, another noncoding CDWL is working synchronously and pointing at the same direction. The spatial and temporal resolution are 19.2 m and 2 s, respectively. This noncoding CDWL is upgraded from our previous system [24].

In order to test the high range resolution of the Golay coding CDWL, the system is pointed at a building. The distance is measured as 1045.5 m away by a ranging lidar. Figure 4(a) is the power spectrum distribution from the atmosphere and the building. As shown in Fig. 4(b), the power spectrum at 1044 m (corresponding to the 174th range bin) is higher than that in neighboring bins. The enlarged power spectrum of the hard target is shown in Fig. 4(c); the blue circle is the raw power spectrum data, and the line is its Gaussian fitting curve. The fitting center is 80.03 ± 0.05 MHz. The Doppler frequency shift is 0, indicating no relative speed between the lidar and the building. As shown in Fig. 4(c), because a rectangle window function is used in FFT, the corresponding sinc function will induce two sidelobes beside the Gaussian curve. However, the influence of sidelobes on the wind retrieval is negligible, demonstrating the effect of the feedback loop.

For comparison, the atmosphere backscattering power spectra from the Golay coding CDWL and noncoding CDWL are plotted in Fig. 5. The intensity of power spectrum of the noncoding CDWL is higher than that of coding CDWL, due to its higher EDFA power and longer spatial resolution. The detailed power spectra at a distance around 100 m, 300 m, and 500 m are plotted from Figs. 5(c) to 5(e), respectively. The Golay coding technique results in a spectral broadening of the signal, resulting in lower CNR. The distance is not exactly same because of the different spatial resolutions of the two lidars. The power spectra of noncoding CDWL are plotted with circles while that of coding CDWL are lines. The narrower pulse duration broadens the FWHM of the power spectra. The sidelobes can be seen, which are introduced by the rectangle window. Due to the fluctuation of the transmitted laser, the substations in Eq. (5) will introduce negative values; so, the intensity of the decoded power spectra may be less than 0.

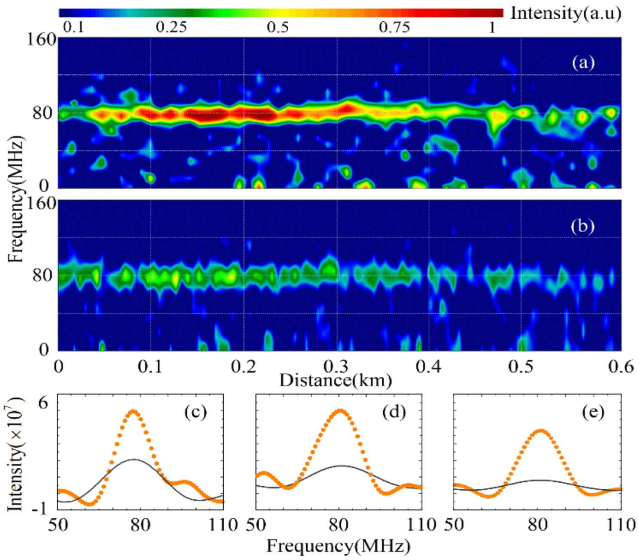

Fig. 5. Power spectra of Golay coding CDWL and noncoding CDWL. (a) Power spectra distribution of noncoding CDWL; (b) power spectra distribution Golay coding CDWL; (c) raw power spectra at around 100 m; the circle is the power spectra of noncoding CDWL, and the line is that of coding CDWL. (d) Raw power spectra at around 300 m; (e) raw power spectra at around 500 m.

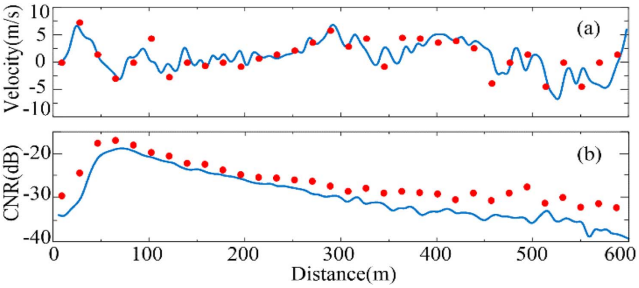

Fig. 6. Radial wind velocity profiles and corresponding CNR of the Golay coding CDWL and noncoding CDWL. (a) The radial wind velocity profiles; blue line is the result of the Golay coding CDWL while the rad point is that of the noncoding CDWL; (b) corresponding CNR distributions of Fig. 6(a).

The intensity of those three power spectra differ greatly, but still can be used to retrieve the wind velocity.

The radial wind velocity is retrieved from the power spectrum by using Gaussian fitting at each bin, as illustrated in Fig. 4(c). Radial wind profiles are shown in Fig. 6(a), and the corresponding CNR distributions are shown in Fig. 6(b). The radial wind velocity profiles from the two CDWLs have the same trend. Benefitting from the better spatial resolution, more details of the wind profile can be seen from the Golay coding CDWL. The CNR of the Golay coding CDWL within 550 m is above −35 dB.

In conclusion, the Golay coding technology is applied in a CDWL, which enhances the spatial resolution of the CDWL. A comparison experiment is carried out between the Golay coding CDWL and noncoding CDWL, and the results show good agreement. There are some problems to be resolved. For example, the Golay coding CDWL demonstrated here is a prototype system, and the measured data were stored in a hard disk, which cannot be processed in real time. In future work, a real-time data processing method based on hardware will be developed. The average power of the fiber laser in this experiment is around 1 W, far lower than the cutting-edge commercial laser. A laser with larger power will be adopted to improve the performance of the Golay coding CDWL.

REFERENCES

1. F. Proctor and D. Hamilton, in *47th AIAA* (2009), paper 344.
2. N. S. Prasad, R. Sibell, S. Vetorino, R. Higgins, and A. Tracy, Proc. SPIE **9465**, 94650C (2015).
3. H. Inokuchi, M. Furuta, and T. Inagaki, in *Proceedings of 29th Congress of the International Council of the Aeronautical Sciences* (2014).
4. A. Dolfi-Bouteyre, G. Canat, M. Valla, B. Augere, C. Besson, D. Goular, L. Lombard, J. Cariou, A. Durecu, D. Fleury, L. Bricteux, S. Brousmiche, S. Lugan, and B. Macq, IEEE J. Sel. Top. Quantum Electron. **15**, 441 (2009).
5. L. P. Thobois, R. Krishnamurthy, S. Loaec, J. P. Cariou, A. Dolfi-Bouteyre, and M. Valla, in *7th AIAA* (2015).
6. D. A. Smith, M. Harris, A. S. Coffey, T. Mikkelsen, H. E. Jørgensen, J. Mann, and R. Danielian, Wind Energy **9**, 87 (2006).
7. M. Shangguan, H. Xia, C. Wang, J. Qiu, S. Lin, X. Dou, Q. Zhang, and J. Pan, Opt. Lett. **42**, 3541 (2017).
8. C. J. OConnor and D. K. Rutishauser, "Enhanced airport capacity through safe, dynamic reductions in aircraft separation: NASA's Aircraft Vortex Spacing System (AVOSS)," NASA technical report, 2001.
9. R. G. Frehlich and M. J. Kavaya, Appl. Opt. **30**, 5325 (1991).
10. H. A. Al-Asadi, M. H. Al-Mansoori, S. Hitam, M. I. Saripan, and M. A. Mahdi, Opt. Express **19**, 1842 (2011).
11. R. G. Smith, Appl. Opt. **11**, 2489 (1972).
12. M. Levin, IEEE Trans. Inf. Theory **11**, 100 (1965).
13. C. Besson, A. Dolfi-Bouteyre, G. Canat, N. Cézard, B. Augère, A. Durecu, L. Lombarb, M. Valla, and A. Hallermeyer, Aerosp. Lab **12**, 1 (2016).
14. L. Lombard, M. Valla, C. Planchat, D. Goular, B. Augère, P. Bourdon, and G. Canat, Opt. Lett. **40**, 1030 (2015).
15. L. Lombard, A. Dolfi-Bouteyre, C. Besson, B. Augère, P. Bourdon, A. Durécu, D. Goular, J. Le Gouët, C. Planchat, W. Renard, M. Valla, and G. Canat, Proc. SPIE **9645**, 96450B (2015).
16. N. S. Prasad, in *Atmospheric and Space Environments Conference* (2018), paper 2863.
17. J. King, D. Smith, K. Richards, P. Timson, R. Epworth, and S. Wright, J. Lightwave Technol. **5**, 616 (1987).
18. M. Nazarathy, S. A. Newton, R. P. Giffard, D. S. Moberly, F. Sischka, W. R. Trutna, and S. Foster, J. Lightwave Technol. **7**, 24 (1989).
19. F. Yang, Y. He, W. Chen, and Y. Zhan, IEEE Photon. Technol. Lett. **26**, 2337 (2014).
20. A. Seleym, in *ICNS 4C3* (2016).
21. Y. Mao, N. Guo, K. L. Yu, H. Y. Tam, and C. Lu, IEEE Photon. J. **4**, 2243 (2012).
22. F. Wang, C. Zhu, C. Cao, and X. Zhang, Opt. Express **25**, 3504 (2017).
23. M. A. Soto, G. Bolognini, and F. Di Pasquale, Opt. Lett. **36**, 232 (2011).
24. C. Wang, H. Xia, M. Shangguan, Y. Wu, L. Wang, L. Zhao, J. Qiu, and R. Zhang, Opt. Express **25**, 20663 (2017).